Münchener Abhandlungen
zum Alten Orient 6

Kai Kaniuth (ed.)

Karacamirli — Tepe 5
A multi-period necropolis in Western Azerbaijan

with contributions by
Andrei Asăndulesei, Florian Becker, Jörg W.E. Fassbinder,
Andrea Göhring, Martin Gruber, Gisela Grupe, Stefan Hölzl,
Michael Joachimski, Christoph Mayr and Michaela Schauer



PeWe-Verlag

Münchener Abhandlungen zum Alten Orient
Band 6

Münchener Abhandlungen zum Alten Orient

herausgegeben von

Adelheid Otto

unter Mitarbeit von

Ursula Calmeyer-Seidl

Berthold Einwag

Michael Herles

Kai Kaniuth

Simone Mühl

Michael Roaf

Elisa Roßberger

Karacamirli — Tepe 5
A multi-period necropolis in Western Azerbaijan

edited by
Kai Kaniuth

with contributions by Andrei Asăndulesei, Florian Becker,
Jörg W.E. Fassbinder, Andrea Göhring, Martin Gruber, Gisela Grupe,
Stefan Hölzl, Michael Joachimski, Christoph Mayr and Michaela Schauer



PeWe-Verlag
2020

Gedruckt mit Unterstützung der Fritz Thyssen Stiftung.

Bibliografische Information der Deutschen Nationalbibliothek
Die Deutsche Nationalbibliothek verzeichnet diese Publikation in der Deutschen Nationalbibliografie; detaillierte bibliografische Daten sind im Internet über http://dnb.dnb.de abrufbar.

© PeWe-Verlag – Gladbeck 2020

Alle Rechte, insbesondere das Recht der Vervielfältigung und Verbreitung sowie der Übersetzung, vorbehalten. Kein Teil des Werkes darf in irgendeiner Form durch Fotokopie, Mikrofilm usw. ohne schriftliche Genehmigung des Verlages reproduziert oder unter Verwendung elektronischer Systeme verarbeitet, vervielfältigt oder verbreitet werden.

Layout und Prepress: Martin Gruber, München/Berlin
Umschlaggestaltung: PeWe-Verlag, Gladbeck
Umschlagabbildung: Bronze Disks 0179 and 0180 from Burial 9 of Karacamirli, Tepe 5 © Martin Gruber

Druck und Verarbeitung: Memminger MedienCentrum
Gedruckt auf alterungsbeständigem Papier

Printed in Germany

ISBN: 978-3-68985-017-3

In Memory of
İlyas Babayev (1935–2017)



Gurban Tepe, August 2017

Table of Contents

List of Figures XI

List of Tables XIX

Preface XXI

I. Introduction to the volume 1
Kai Kaniuth

I.1 The site of Tepe 5 3
I.2 The organization of the present volume 5

II. The Geophysical Prospection around Tepe 5 7
Jörg W. E. Fassbinder, Florian Becker, Andrei Asăndulesei

II.1 Introduction 7
II.2 The Geophysical Prospection of Tepe 5 9
II.3 Conclusion 13

III. The Chalcolithic Pits 15
Martin Gruber

III.1 Pit KG-016/KG-019 15
III.2 Pit-KG-049 17
III.3 The Chalcolithic pottery in Pit-Complexes A and B 17
III.4 Dating 19
III.5 Conclusions 26

IV. The Tepe 5 Cemetery 29
Martin Gruber

IV.1 Introductory remarks 29
IV.2 Late Bronze/Early Iron Age 32
IV.2.1 A short history of research 32
IV.2.2 The Khojaly-Gadabay-Culture 33
IV.2.3 General description of burials and grave contents 35
IV.2.4 Radiocarbon dates 39
IV.2.5 The sequence of Late Bronze/Early Iron Age burials at Tepe 5 40
IV.3 Late Antique Period 41

IV.3.1 Historical background 41
IV.3.2 Regional context 42
IV.3.3 General description of burials and grave contents 43
IV.3.4 Radiocarbon dates 46
IV.4 Medieval Period 46
IV.4.1 Historical background 46
IV.4.2 Regional context 47
IV.4.3 General description of the burials 49
IV.4.4 Radiocarbon dates 51
IV.5 Undated burials 52
IV.6 Pit-Complexes 53
IV.6.1 Pit-Complex A 54
IV.6.2 Pit-Complex B 54
IV.6.3 Pit-Complex C 55
IV.7 KG-100 and KG-101 56
IV.8 Stray finds 57
IV.9 Detailed description of the burials 60

V. Morphological and histological survey of human remains from Tepe 5 163
Andrea Göhring

V.1 Introduction 163
V.2 Methods 163
V.2.1 Morphological analysis 163
V.2.2 Histological analysis 168
V.2.3 X-ray analysis 170
V.2.4 Data analysis and software 170
V.3 Catalogue of human remains 170
V.3.1 Late Bronze Age/Early Iron Age burials 170
V.3.2 Late Antique burials 176
V.3.3 Medieval Burials 183
V.3.4 Undated burials 200
V.4 Morphological results and discussion 202
V.4.1 State of preservation 202
V.4.2 Age and sex distribution 202
V.4.3 Osteometry 204
V.4.3.1 Cranial measurements 204
V.4.3.2 Postcranial measurements 209
V.4.4 Joint status 211
V.4.5 Pathological alterations of bones and teeth 212
V.4.6 Acquired and epigenetic non-metric variants of bones 214
V.5 Summary 216

VI. Multi-isotope fingerprint of humans, animals, and environmental samples from Karacamirli 217
Andrea Göhring, Stefan Hölzl, Michael Joachimski, Christoph Mayr, Gisela Grupe

VI.1 Introduction 217
VI.2 Material and Methods 220
VI.2.1 Material 220
VI.2.2 Extraction of collagen and apatite and mass spectrometry 220
VI.2.2.1 Extraction and measurement of $\delta^{13}C_{collagen}$ and $\delta^{15}N_{collagen}$ of bone collagen 220
VI.2.2.2 Extraction and measurement of $\delta^{13}C_{carbonate}$ and $\delta^{18}O_{carbonate}$ of bone apatite 222
VI.2.2.3 Extraction and measurement of $\delta^{18}O_{phosphate}$ of bone apatite 222
VI.2.2.4 Extraction and measurement of $^{87}Sr/^{86}Sr$ of bones, teeth, and environmental samples 223
VI.2.3 Data analysis 223
VI.3 Results 225
VI.3.1 Diet reconstruction 225
VI.3.2 Assessment of the places of origin 230
VI.3.3 Cluster analysis 233
VI.4 Discussion 237
VI.5 Conclusion 242

VII. Portable X-ray Analysis 245
Michaela Schauer

VII.1 Geological background 246
VII.1.1 Geology of the Caucasus and Azerbaijan 246
VII.1.2 Geology of the Ganja-Qazakh region 248
VII.1.3 The Location of Tepe 5 251
VII.1.4 Soil samples 251
VII.1.4.1 Dataset 253
VII.1.4.2 Comments on the chemistry 255
VII.2 Pottery 256
VII.2.1 The Pottery of Tepe 5 257
VII.2.1.1 Results of p-XRF analyses 257
VII.2.1.2 Chemical groups and related fabric types (Martin Gruber, Kai Kaniuth) 276
VII.2.1.3 The pottery of Tepe 5 through time 278
VII.3 Obsidian 282
VII.3.1 Sources 282

VII.3.2 The obsidian from Tepe 5 286
VII.4 Metal analyses 287
VII.4.1 Copper 292
VII.4.2 Arsenical Copper 292
VII.4.3 Tin Bronze 292
VII.4.4 Iron 293
VII.4.5 Silver 293
VII.4.6 Summary 293
VII.5 Conclusion 293

VIII. Summary 295
Kai Kaniuth

IX. List of contexts 299

X. List of finds 303

XI. Bibliography 311

List of Figures

Unless otherwise indicated the copyright of figures and drawings lies with the individual authors. All drawings by Manfred Lercнl are labelled [ml].

Fig. 1. Archaeological sites (blue and red) and obsidian deposits (green) mentioned in this volume 1
Fig. 2. Archaeological sites north of Garajamirli 2
Fig. 3. Survey grid showing Tepe 5 in relation to Gurban Tepe and other archaeological sites of Karacamirli 3
Fig. 4. Location of Tepe 5 on a satellite image (© Quickbird, April 12, 2007) 4
Fig. 5. Karacamirli. Satellite overview of the total area overlaid by the grey scale images of the magnetometer survey areas (Quickbird imagery © 2013 DigitalGlobe from April 12th, 2007) ... 7
Fig. 6. Karacamirli. Tepe 5 area: Quickbird satellite image from April 12th 2007 (© 2013 DigitalGlobe); WGS 84 UTM 38N 8
Fig. 7. Karacamirli. Tepe 5 area: Quickbird Satellite image from 2007 (© 2013 DigitalGlobe), overlaid by the magnetogram of the area. The location of former and still existing mounds is marked in yellow; WGS 84 UTM 38N 9
Fig. 8. Karacamirli. Tepe 5 and its surroundings: Magnetogram of the burials and mounds, the »inner enclosure« and its periphery 10
Fig. 9. Karacamirli, Tepe 5. Detail of the magnetogram with the burial mound 11
Fig. 10. Karacamirli, Tepe 5. Detail of the magnetogram 12
Fig. 11. Karacamirli, Tepe 5. Detail of the magnetogram (30 % overlay by inverted high-pass filtered data) overlaid by photogrammetric image of the excavation (© Martin Gruber) ... 13
Fig. 12. Detail of the fill of pit KG-016. The transition from light to dark brown soil in the west marks the edge of the pit 15
Fig. 13. Location of the Chalcolithic pits on Tepe 5 16
Fig. 14. Finds from pit KG-016 [ml] 17
Fig. 15. Selected pottery from pit KG-016 [ml] 20
Fig. 16. Selected pottery from Chalcolithic contexts (KG-016-0045, KG-049-0196, KG-022-0073 and KG-023–0082) [ml] 21
Fig. 17. Selected pottery from pit KG-016 22
Fig. 18. Selected pottery from pit KG-016 23
Fig. 19. Selected pottery from contexts KG-016 and KG-018 23
Fig. 20. Cross-section of a sherd (0045-01) revealing the impressions of two jointed slabs 23
Fig. 21. Contour map of Tepe 5 with orthophotos of the excavated area 29
Fig. 22. Location of burials and Pit-Complexes on Tepe 5 30
Fig. 23. Temporary southern section of the south-western quadrant of square 6300/7990 showing the three natural layers on Tepe 5; the eastern part (right side) was disturbed by the grave-pit of the Medieval Burial 38 31
Fig. 24. Radiocarbon dates showing the three occupation phases of the cemetery 31
Fig. 25. Proposed subdivision of the Late Bronze/Early Iron Age (Khojaly-Gadabay-Culture) in north-western Azerbaijan after Минкевич-Мустафаева 1962, Гусейнова 1989; 2011 and Погребова 2011 33
Fig. 26. Punctate ornamentation on pot 0200-03 from Burial 2 34
Fig. 27. Location of Late Bronze/Early Iron Age burials 36
Fig. 28. Orientation of the grave-pits and skeletons in the Late Bronze/Early Iron Age 37
Fig. 29. Radiocarbon dates of Late Bronze/Early Iron Age burials 39
Fig. 30. Proposed chronological sequence of Late Bronze/Early Iron Age burials 40
Fig. 31. Location of Late Antique burials 42
Fig. 32. Orientation of the grave-pits and skeletons in the Late Antique period 44
Fig. 33. Typical black coloured stains on a Late Antique vessel from Burial 25 (0209-01) 44
Fig. 34. Radiocarbon dates of Late Antique burials 45
Fig. 35. Location of Medieval burials 47

Fig. 36. Burial 29 (KG-031) with an individual placed on its right side (first group)....49
Fig. 37. Burial 37 (KG-052) with an individual laying on its back with stretched legs (second group)....50
Fig. 38. Orientation of the grave-pits and skeletons in the Medieval period....50
Fig. 39. Radiocarbon dates of Medieval burials....51
Fig. 40. Undated Burial 42 (KG-035) with an infant individual....52
Fig. 41. Location of undated burials....53
Fig. 42. Plan of Pit-Complex A....54
Fig. 43. Plan of Pit-Complex B....55
Fig. 44. Plan of Pit-Complex C....56
Fig. 45. Pit-Complex C with Burial 21 (KG-074) and remains of Burial 1 (KG-094)....56
Fig. 46. Distribution of stray finds....57
Fig. 47. Stray finds (KG-024) [ml]....58
Fig. 48. Plan of Burial 1 (KG-094); Pit-Complex C-3....61
Fig. 49. Black-polished pot KG-094-0425-01 from Burial 1 with punctate ornamentation....62
Fig. 50. Black-polished bowl KG-094-0425-03 from Burial 1....62
Fig. 51. Pottery from Burial 1 (KG-094) [ml]....63
Fig. 52. Pottery from the fill of Burial 1 (KG-094) [ml] 63
Fig. 53. Finds from the fill of Burial 1 (KG-094) [ml]... 64
Fig. 54. Distribution of beads and obsidian flakes in the fill of Burials 1 (KG-094) and 21 (KG-074). 64
Fig. 55. Light blue frit bead (0453) with a cylindrical body and three applied knobs....65
Fig. 56. Black-polished pot with punctate ornamentation (0200-04) from Burial 2 (KG-044)....67
Fig. 57. Black-polished bowl (0200-07) from Burial 2 (KG-044)....67
Fig. 58. Plan of Burial 2 (KG-044)....68
Fig. 59. Pottery from Burial 2 (KG-044) [ml]....69
Fig. 60. Walnut-shaped bowl (0200-02) from Burial 2 (KG-044)....70
Fig. 61. Plan of Burial 3 (KG-051)....72
Fig. 62. Pottery from Burial 3 (KG-051) [ml]....72
Fig. 63. Pit-Complex A with Burials 4 (KG-039 & KG-040) and 5 (KG-038)....73
Fig. 64. Plan of Burials 4 (KG-039 & KG-040) and 5 (KG-038); Pit-Complex A....74
Fig. 65. Finds from Burial 4 (KG-039 & KG-040) [ml]..75
Fig. 66. Finds from Burial 5 (KG-038) [ml]....76
Fig. 67. Pit-Complex C-1 and 2 with Burial 6 (KG-095-0497) in the south, Burial 45 (KG-096) in the west and Burial 22 (KG-095-0496) in the north....77
Fig. 68. Plan of Burials 6 (KG-095-0497), 22 (KG-095-0496) and 45 (KG-096); Pit Complex C-1–2....78
Fig. 69. Finds from Burial 6 (KG-095-0497) [ml]....79
Fig. 70. Bowl 0498-01 from Burial 6 (KG-095-0497)....79
Fig. 71. Pot 0498-02 with decorated lug from Burial 6.79
Fig. 72. Pottery from Burial 6 (KG-095-0497) [ml]....80
Fig. 73. Pot 0498-03 with polished decoration and disc-shaped lug from Burial 6 (KG-095-0497). 81
Fig. 74. Pot 0498-06 from Burial 6 (KG-095-0497) with circular impressions on the shoulder....81
Fig. 75. Pit-Complex A with Burial 7 (KG-026) and the Medieval Burial 28 (KG-027)....84
Fig. 76. Pottery from Burial 7 (KG-026) [ml]....84
Fig. 77. Plan of Burial 7 (KG-026); Pit-Complex A....85
Fig. 78. Black-polished pot 0100-03 from Burial 7 (KG-026)....86
Fig. 79. Fragment of pot 0100-01 from Burial 7 (KG-026)....86
Fig. 80. Black-polished bowl 0100-02 from Burial 7 (KG-026)....86
Fig. 81. Pot 0100-09 from Burial 7 (KG-026)....86
Fig. 82. Pottery from the fill of Burial 7 (KG-026) [ml]....86
Fig. 84. Pit KG-057 with remains of Burial 8 in the south-eastern (pot 0417-01) and north-western corner (KG-057-0247 and KG-057-0404 with one half of bowl 0418-01), and the Late Antique Burials 23 (KG-057-0415) and 24 (KG-057-0414)....88
Fig. 83. Grey coloured pot 0417-01 from Burial 8 (KG-057-0247 and KG-057-0404)....88
Fig. 85. The rejoined halves of bowl 0418-01 (Burial 8) and 0241-02 (fill of Burial 15)....89
Fig. 86. Pottery from Burial 8 (KG-057-0247 & KG-057-0404) [ml]....89
Fig. 87. Plan of the remains of Burial 9 (KG-043)....90
Fig. 88. Bronze objects and adornment of the individual in Burial 9 (KG-043)....91
Fig. 89. Ornamented bronze discs (0179 and 0180) *in situ* with remains of a human skull in between....91
Fig. 90. Finds from Burial 9 (KG-043) [ml]....92
Fig. 91. Finds from Burial 9 (KG-043) [ml]....93
Fig. 92. Grey coloured pot (0164-02) from Burial 10 (KG-041)....94
Fig. 93. Grey coloured cup (0164-01) from Burial 10 (KG-041)....94
Fig. 94. Pottery from Burial 10 (KG-041) [ml]....94
Fig. 95. Plan of Burials 10 (KG-041) and 11 (KG-029); Pit-Complex A....96
Fig. 96. Grey coloured jug (0112-01) from Burial 11 (KG-029)....97
Fig. 97. Grey coloured churn (0112-02) from Burial 11 (KG-029)....97

Fig. 98. Pottery from Burial 11 (KG-029) [ml] 98
Fig. 99. Plan of Burial 12 (KG-064) 99
Fig. 100. Pottery from Burial 12 (KG-064) [ml] 100
Fig. 101. Plan of Burial 13 (KG-032) 100
Fig. 102. Burial 13 (KG-032) 101
Fig. 103. Finds from Burial 13 (KG-032) [ml] 101
Fig. 104. Pot 0144-01 from Burial 13 (KG-032) 101
Fig. 105. Pottery from Burial 13 (KG-032) [ml] 102
Fig. 106. Pot 0144-02 from Burial 13 (KG-032) 103
Fig. 107. Pot 0144-04 from Burial 13 (KG-032) 103
Fig. 108. Small beaker 0144-05 from Burial 13 (KG-032) 103
Fig. 109. Pottery from Burial 14 (KG-059) [ml] 105
Fig. 110. Plan of Burial 14 (KG-059) 106
Fig. 111. Pot 0252-01 from Burial 14 (KG-059) 107
Fig. 112. Finds from Burial 14 (KG-059) [ml] 107
Fig. 113. Carnelian beads from Burial 14 (KG-059) [ml] 108
Fig. 114. Frit beads and other finds from Burial 14 (KG-059) [ml] 109
Fig. 115. Plana A and B of Burial 15 (KG-058); Pit-Complex B 114
Fig. 116. Bowl 0241-03 from Burial 15 (KG-058) 115
Fig. 117. Bowl 0241-04 from Burial 15 (KG-058) 115
Fig. 118. Bowl 0241-01 from Burial 15 (KG-058) 115
Fig. 119. Pottery from Burial 15 (KG-059) [ml] 116
Fig. 120. Small pot 0241-05 from Burial 15 (KG-058) 117
Fig. 121. Pot 0241-07 from Burial 15 (KG-058) 117
Fig. 122. Finds from Burial 15 (KG-059) [ml] 118
Fig. 123. Plan of Burial 16 (KG-055) 120
Fig. 124. Pottery and finds from Burial 16 (KG-065) [ml] 120
Fig. 125. Jug 0221-01 from Burial 16 (KG-055) 120
Fig. 126. Pottery from Burial 17 (KG-065) [ml] 121
Fig. 127. Plan of Burial 18 (KG-015) 121
Fig. 128. Pottery from Burial 18 (KG-015) [ml] 122
Fig. 129. Plan of Burial 19 (KG-063) 122
Fig. 130. Finds from Burial 19 (KG-063) [ml] 123
Fig. 131. Plan of Burial 20 (KG-030 & KG-102); Pit-Complex A 123
Fig. 132. Plan of Burial 21 (KG-074); Pit-Complex C-3–4 124
Fig. 133. Finds from Burial 21 (KG-074) that probably originate from Burial 1 (KG-094) [ml] 125
Fig. 134. Trefoil jug 0506-01 from Burial 21 (KG-074) 125
Fig. 135. Pottery from Burial 21 (KG-074) [ml] 125
Fig. 136. Find from Burial 21 (KG-074) [ml] 126
Fig. 137. Two-handled pot (0419-01) from Burial 23 127
Fig. 138. Plan of Burials 8 (KG-057-0247 & KG-057-0404), 23 (KG-057-0415) and 24 (KG-057-0414); Pit-Complex B 128
Fig. 139. Pottery from Burial 23 (KG-057-0415) [ml] 129
Fig. 140. Distribution of finds in the fill of pit KG-057 (Pit-Complex B) 129
Fig. 141. Finds from the fill of pit KG-057 (Pit-Complex B) [ml] 130
Fig. 142. Burial 25 (KG-053) 132
Fig. 143. Plan of Burial 25 (KG-053) 133
Fig. 144. Finds from Burial 25 (KG-053) [ml] 134
Fig. 145. Pottery from Burial 25 (KG-053) [ml] 134
Fig. 146. Plan of Burial 26 (KG-066) 135
Fig. 147. Burial 26 (KG-066) 136
Fig. 148. Pottery from Burial 26 (KG-066) [ml] 136
Fig. 149. Pottery from Burial 27 (KG-097) [ml] 136
Fig. 150. Plan of Burial 27 (KG-097) 137
Fig. 151. Burial 27 (KG-097) 138
Fig. 152. Burial 27 Finds from Burial 27 (KG-097) [ml] 138
Fig. 153. Plan of Burial 28 (KG-027); Pit-Complex A 139
Fig. 154. Plan of Burial 29 (KG-031) with bronze object (0123) 140
Fig. 155. Burial 30 (KG-036) 141
Fig. 156. Plan of Burial 30 (KG-036) 142
Fig. 157. Burial 31 (KG-042) 143
Fig. 158. Plan of Burial 31 (KG-042) 144
Fig. 159. Plan of Burial 32 (KG-045) 145
Fig. 160. The southern part of Burial 33 (KG-046) in 2017 146
Fig. 161. Plan of Burial 33 (KG-046) 147
Fig. 162. Burial 34 (KG-048) and parts of the pottery inventory of Burial 2 (KG-044) 148
Fig. 163. Plan of Burial 34 (KG-048) 149
Fig. 164. Plan of Burial 35 (KG-047 & KG-098) 150
Fig. 165. Burial 36 (KG-050) 151
Fig. 166. Plan of Burial 36 (KG-050) 152
Fig. 167. Burial 38 (KG-073) 153
Fig. 168. Plan of Burial 37 (KG-052) 154
Fig. 169. Plan of Burial 38 (KG-073) 155
Fig. 170. Finds from Burial 38 (KG-073) [ml] 155
Fig. 171. Plan of Burials 39 (KG-077) and 43 (KG-076) 156
Fig. 172. Find from Burial 39 (KG-077) [ml] 157
Fig. 173. Burials 39 (KG-077) and 43 (KG-076) 157
Fig. 174. Plan of Burial 40 (KG-089) 158
Fig. 175. Plan of Burial 41 (KG-093) 159
Fig. 176. Burial 41 (KG-093) 160
Fig. 177. Plan of Burial 42 (KG-035) 160
Fig. 178. Plan of Burial 44 (KG-092) 161
Fig. 180. Example of the histological composition of bone in a young individual. Histological thin section of a femur diaphysis sample of individual KG-095-0496, Burial 22 (photograph by A. Alesi) 168
Fig. 181. Example of the histological composition of bone in a young individual. Histological thin section of a femur diaphysis sample

of individual KG-095-0496, Burial 35 (photograph by A. Alesi) 168
Fig. 182. Example of the histological composition of bone in a mature or senile individual. Histological thin section of a femur diaphysis sample (periosteal part) of individual KG-092-0398, Burial 44 (photograph by A. Alesi) 169
Fig. 183. Example of the TCA analysis of a tooth in an adult or mature individual. Histological thin section of an upper premolar sample of individual KG-097-0455, Burial 27 (photograph by A. Alesi)..... 169
Fig. 184. Example of the TCA analysis of a tooth in a mature or senile individual. Histological thin section of a lower premolar sample of individual KG-090-0398, Burial 44 (photograph by A. Alesi)..... 169
Fig. 185. Skeletal scheme of KG-094-0474 (Burial 1).....171
Fig. 186. Skeletal scheme of KG-039-0163 and KG-040-0165 (Burial 4) 171
Fig. 187. Skeletal scheme of KG-038-0146 (Burial 5)..... 172
Fig. 188. Norma frontalis of the skull of individual KG-026-0105 (Burial 7)..... 172
Fig. 189. Norma lateralis of the skull of individual KG-026-0105 (Burial 7)..... 172
Fig. 190. Skeletal scheme of individual KG-095-0497 (Burial 6) 173
Fig. 191. Skeletal scheme of individual KG-026-0105 (Burial 7) 173
Fig. 192. Skeletal scheme of KG-057-0247 and KG-057-0404 (Burial 8) 174
Fig. 193. Skeletal scheme of KG-032-0166 (Burial 13) ... 175
Fig. 194. Healed rib fracture (see arrows) on a right rib of individual KG-032-0166 (Burial 13) 175
Fig. 195. Skeletal scheme of KG-058-0243 (Burial 15)... 175
Fig. 196. Skeletal scheme of KG-030-0113 and KG-102-0491 (Burial 20) 176
Fig. 197. Skeletal scheme of KG-095-0496 (Burial 22) .. 176
Fig. 198. Skeletal scheme of KG-074-0507 (Burial 21)....177
Fig. 199. Skeletal scheme of KG-057-0415 (Burial 23) 177
Fig. 200. Lambdoid ossicles (see arrows) at the Sutura lambdoidea of individual KG-057-0415 (Burial 23)..... 178
Fig. 201. Ossicle at the lambda and lambdoid ossicles (see arrows) at the Sutura lambdoidea of individual KG-057-0415 178
Fig. 202. Canalis condylaris patent at the right side of the Foramen magnum (see arrow) of individual KG-057-0415 (Burial 23) 178
Fig. 203. Skeletal scheme of KG-057-0414 (Burial 24)... 179
Fig. 204. Osteomyelitis (see arrows) at the anterior-lateral side of the left tibia of individual KG-057-0414 (Burial 24)..... 179
Fig. 205. Periostitis on the anterior side of the left tibia of individual KG-053-0208 (Burial 25)... 179
Fig. 206. Skeletal scheme of KG-053-0208 (Burial 25) .. 180
Fig. 207. Lambdoid ossicles at the Sutura lambdoidea of individual KG-053-0208 (Burial 25)..... 180
Fig. 208. Norma frontalis of the skull of individual KG-053-0208 (Burial 25) 180
Fig. 209. Norma lateralis of the skull of individual KG-053-0208 (Burial 25) 181
Fig. 211. Skeletal scheme of KG-066-0392 (Burial 26) ...181
Fig. 210. Healed fracture (see arrows) of the posterior part of the left ulna of individual KG-066-0392 (Burial 26).....181
Fig. 212. Skeletal scheme of KG-097-0455 (Burial 27)... 182
Fig. 213. Foramen transversum bipartitum (see upper arrow) as well as Processus spinosus bipartitus (see lower arrow) on the sixth cervical vertebra of individual KG-097-0455 (Burial 27) 182
Fig. 214. Norma occipitalis of the skull of individual KG-097-0455 (Burial 27) with an ossicle at the lambda (see arrows)..... 182
Fig. 215. Skeletal scheme of KG-027-0106 (Burial 28) ... 183
Fig. 216. Anterior-lateral view on the right tibia of individual KG-027-0106 (Burial 28) with an osteomyelitis at the proximal part of the bone shaft including a central sisus (cloaca) for pus drainage. The central sisus (cloaca) and the coarsely woven bone at the cortex are clearly visible 183
Fig. 217. Lateral view on the right tibia of individual KG-027-0106 (Burial 28) with an osteomyelitis at the proximal part of the bone shaft. The coarsely woven bone at the cortex and consequent thickening of the bone are clearly visible 183
Fig. 218. X-ray Image (10 mAs, 52 kVp) of the proximal part of the right tibia of individual KG-027-0106 (Burial 28) from anterior (left) and lateral (right).....184
Fig. 219. Cribra orbitalia (see arrows) in the right and left orbit of individual KG-031-0120 (Burial 29).....184
Fig. 220. Exsutural Foramen mastoideum (see arrow) on the left side of the skull of individual KG-031-0120 (Burial 29).....184
Fig. 221. Skeletal scheme of KG-031-0120 (Burial 29) ... 185
Fig. 222. Processi spinosi bipartiti (see arrows) on cervical vertebrae C3–C6 of individual KG-031-0120 (Burial 29)..... 185

Fig. 223. Foramen transversum bipartitum (see arrrow) on the right side of cervical vertebra C7 of individual KG-031-0120 (Burial 29)..... 185
Fig. 224. Norma frontalis of the skull of individual KG-031-0120 (Burial 29)..... 186
Fig. 225. Norma lateralis of the skull of individual KG-031-0120 (Burial 29)..... 186
Fig. 226. Doubled Foramen zygomaticofaciale (see arrows) on the left Os zygomaticum of individual KG-036-0134 (Burial 30)..... 186
Fig. 227. Skeletal scheme of KG-036-0134 (Burial 30)... 187
Fig. 228. Norma frontalis of the skull of individual KG-036-0134 (Burial 30)..... 187
Fig. 229. Norma lateralis of the skull of individual KG-036-0134 (Burial 30)..... 187
Fig. 230. Skeletal scheme of KG-042-0173 (Burial 31).... 188
Fig. 231. Skeletal scheme of KG-045-0193 (Burial 32)... 188
Fig. 232. Skeletal scheme of KG-046-0192 (Burial 33)... 189
Fig. 233. Norma frontalis of the skull of individual KG-046-0192 (Burial 33)..... 189
Fig. 234. Norma lateralis of the skull of individual KG-046-0192 (Burial 33)..... 189
Fig. 235. Skeletal scheme of KG-048-0197 (Burial 34)... 190
Fig. 236. Bony spurs (see arrows) at the Os ischii projecting in the Foramen obturatum of the right pelvis of individual KG-038-0197 (Burial 34)..... 190
Fig. 237. Fusion of the second and third cervical vertebrae (see arrows) of individual KG-048-0197 (Burial 34)..... 190
Fig. 238. Supraorbital notches (see arrows above orbits) and accessory Foramina infraorbitalia (see arrows below orbits) on both sides of the facial skull of individual KG-048-0197 (Burial 34)..... 191
Fig. 239. Facies articularis superior atlantis bipartita on the superior side of the atlas of individual KG-048-0197 (Burial 34)..... 191
Fig. 240. Norma frontalis of the skull of individual KG-048-0197 (Burial 34)..... 191
Fig. 241. Norma lateralis of the skull of individual KG-048-0197 (Burial 34)..... 191
Fig. 242. Skeletal scheme of KG-047-0217 and KG-098-0467 (Burial 35)..... 192
Fig. 243. Skeletal scheme of KG-050-0203 (Burial 36).. 193
Fig. 244. Lambdoid ossicles (see arrows) on the Sutura lambdoidea of individual KG-050-0203 (Burial 36)..... 193
Fig. 245. Canalis condylaris on the right side of the Foramen magnum (left arrow) of individual KG-050-0203 (Burial 36), while the canal is not patent on the left side (right arrow)..... 193
Fig. 246. Foramen supratrochleare (see arrows) on the distal end of the left Humerus of individual KG-050-0203 (Burial 36)..... 194
Fig. 247. Norma frontalis of the skull of individual KG-050-0203 (Burial 36)..... 194
Fig. 248. Norma lateralis of the skull of individual KG-050-0203 (Burial 36)..... 194
Fig. 249. Skeletal scheme of KG-052-0205 (Burial 37)... 195
Fig. 250. Foramen transversum bipartitum (see arrows) on two cervical vertebrae (vertebra C4 and C5) of individual KG-052-0205 (Burial 37). The foramina on the fifth vertebra (right) are damaged and only partly visible..... 195
Fig. 251. Norma frontalis of the skull of individual KG-073-0508 (Burial 38)..... 195
Fig. 252. Norma lateralis of the skull of individual KG-073-0508 (Burial 38)..... 195
Fig. 253. Skeletal scheme of KG-073-0508 (Burial 38) .. 196
Fig. 254. Skeletal scheme of KG-077-0517 (Burial 39).... 196
Fig. 255. Skeletal scheme of KG-089-0387 (Burial 40) .. 197
Fig. 256. Osteophytes (see arrows) at the anterior side of four lumbar vertebrae of individual KG-093-0480 (Burial 41)..... 197
Fig. 257. Skeletal scheme of KG-093-0480 (Burial 41) .. 198
Fig. 258. Posterior view on the proximal part of the left tibia of individual KG-093-0480 (Burial 41) with osteophytes (see arrows) at the medial side, probably caused by an injury of the Ligamentum collaterale tibiae..... 198
Fig. 259. Osteophytes (see arrows) at the Facies auricularis of the left pelvis of individual KG-093-0480 (Burial 41)..... 198
Fig. 260. Damage of the right joint (left nd) of the sacrum of individual KG-093-0480 (Burial 41) with relatively large osteophytes (see arrows). The corresponding Facies auricularis of the right pelvis could not be examined..... 198
Fig. 261. Enthesiopathy (lateral) and rhomboid fossae (medial) on both clavicles of individual KG-093-0480 (Burial 41)..... 198
Fig. 262. Variant of Allen's fossa (see arrows) at the femoral neck of the left femur of individual KG-093-0480 (Burial 41)..... 199
Fig. 263. Processus supracondylaris (see arrow) on the posterior side of the left humerus diaphysis of individual KG-093-0480 (Burial 41)..... 199
Fig. 264. Canales condylares (see arrows) present on both sides of the Foramen Magnum of individual KG-093-0480 (Burial 41)..... 199

Fig. 265. Foramen supraorbitale with a vertical septum (see arrows) on the left side of the skull of individual KG-093-0480 (Burial 41)..... 199
Fig. 266. Skeletal scheme of KG-035-0136 (Burial 42).. 200
Fig. 267. Cribra orbitalia (see arrows) on both orbits of individual KG-035-0136 (Burial 42)..... 200
Fig. 268. Foramen transversum bipartitum (see left arrow) as well as Processus spinosus bipartitus (see right arrow) at the sixth cervical vertebra of individual KG-076-0515 (Burial 43)..... 200
Fig. 269. Skeletal scheme of KG-075-0515 (Burial 43)... 201
Fig. 270. Skeletal scheme of KG-092-0398 (Burial 44).. 201
Fig. 271. Osteomyelitis (see arrows) on the distal diaphyseal part of the left radius of individual KG-099-0460 (Burial 46)..... 201
Fig. 272. Skeletal scheme of KG-099-0460 (Burial 46). 202
Fig. 273. Sex distribution of the individuals from Karacamirli separated by ^{14}C dating..... 202
Fig. 274. Distribution of age classes of the individuals from Karacamirli separated by ^{14}C dating.... 204
Fig. 275. Distribution of sex per age class of the individuals from Karacamirli..... 204
Fig. 276. Cranial index and basio-bregmatic longitudinal index of nine individuals from Karacamirli..... 205
Fig. 277. Cranial index and basio-bregmatic transversal index of nine individuals from Karacamirli..... 205
Fig. 278. Basio-bregmatic longitudinal index and basio-bregmatic transversal index of nine individuals from Karacamirli..... 206
Fig. 279. Jugo-frontal index and jugo-mandibular index of seven individuals from Karacamirli. Diagonal: jugo-frontal index = jugo-mandibular index..... 206
Fig. 280. Total facial index and superior facial index of eight individuals from Karacamirli..... 206
Fig. 281. Orbital index and nasal index of nine individuals from Karacamirli..... 206
Fig. 282. Pairwise bivariate plot of the resulting three clusters on the twelve-dimensional craniometry dataset of nine humans from Karacamirli..... 207
Fig. 283. Index platymericus of eight individuals from Karacamirli..... 209
Fig. 284. Index cnemicus of six individuals from Karacamirli..... 210
Fig. 285. Mean estimated body height (after Trotter/Gleser 1958) for seven at least juvenile individuals from Karacamirli. Error bars indicate standard deviations..... 210
Fig. 286. $\delta^{13}C_{collagen}$ and $\delta^{15}N_{collagen}$ values of twelve individuals from Karacamirli differentiated by age, sex, and ^{14}C dating..... 225
Fig. 287. $\Delta\delta^{13}C_{carbonate\text{-}collagen}$ and $\delta^{15}N_{collagen}$ values of twelve individuals from Karacamirli differentiated by age and sex, and ^{14}C dating..... 225
Fig. 288. Diet-adjusted $\delta^{13}C$ and $\delta^{15}N$ of possible food sources and humans from Karacamirli..... 226
Fig. 289. Concentration-weighted mixing model for the humans (green squares) from Karacamirli calculated with SISUS using eight different food sources (red circles)..... 228
Fig. 290. $\delta^{18}O_{carbonate}$ and $\delta^{18}O_{phosphate}$ values of twelve individuals from Karacamirli differentiated by age, sex, and ^{14}C dating..... 231
Fig. 291. $^{87}Sr/^{86}Sr$ values of human bones and teeth (enamel), animal bones and teeth (enamel), as well as modern environmental samples from Karacamirli..... 232
Fig. 292. $\delta^{18}O_{phosphate}$ and $^{87}Sr/^{86}Sr$ values of ten individuals from Karacamirli differentiated by age, sex, and ^{14}C dating..... 233
Fig. 293. Pairwise bivariate plot of the resulting two clusters on the five-dimensional isotopic dataset of the humans from Karacamirli..... 234
Fig. 294. Pairwise bivariate plot of the resulting two clusters on the six-dimensional isotopic dataset ($\delta^{13}C_{collagen}$, $\delta^{15}N_{collagen}$, $\delta^{13}C_{carbonate}$, $\delta^{18}O_{carbonate}$, $\delta^{18}O_{phosphate}$, $^{87}Sr/^{86}Sr_{bone}$) of the humans from Karacamirli..... 236
Fig. 295. Pairwise bivariate plot of the resulting two clusters on the six-dimensional isotopic dataset ($\delta^{13}C_{collagen}$, $\delta^{15}N_{collagen}$, $\delta^{13}C_{carbonate}$, $\delta^{18}O_{carbonate}$, $\delta^{18}O_{phosphate}$, $^{87}Sr/^{86}Sr_{enamel}$) of the humans from Karacamirli..... 237
Fig. 296. Map approximatively indicating the (most probable) regions of origins for the primarily non-local individuals from Karacamirli..... 239
Fig. 297. Tectonic map of the Caucasus (after Vincent et al. 2016: Fig. 1)..... 246
Fig. 298. Physical map of Azerbaijan..... 247
Fig. 299. Geological map of the Ganja-Qazakh region (IHPA NGO 2013: 28 Fig. 1.6)..... 249
Fig. 300. The location of Tepe 5..... 250
Fig. 301. The location of clay samples used in this study..... 251
Fig. 302. The location of clay samples from the vicinity of Tepe 5..... 252
Fig. 303. Tepe 5. Scatterplot of clay samples (n=30) showing SiO_2-Al_2O_3-ratio..... 254
Fig. 304. Tepe 5. Ternary plot of soil samples (n=30) showing Fe_2O_3-, CaO-, and MgO-ratio..... 255

Fig. 305. Tepe 5. Ternary plot of pottery samples (n=30) showing Al_2O_3-, K_2O-, and CaO-ratio 256
Fig. 306. Tepe 5. Scatterplot of Early Chalcolithic pottery samples (n=21) and clay samples (n=20) showing Rb/Sr-ratio 257
Fig. 307. Tepe 5. Scatterplot of Early Chalcolithic pottery samples (n=21) and clay samples (n=20) showing Cr-/Zn-ratio 260
Fig. 308. Tepe 5. Scatterplot of Early Chalcolithic pottery samples (n=21) and clay samples (n=20) showing Fe_2O_3/Zn-ratio 260
Fig. 309. Tepe 5. Scatterplot of Early Chalcolithic pottery samples (n=21) and clay samples (n=20) showing K_2O/CaO-ratio 261
Fig. 310. Tepe 5. Scatterplot of Early Chalcolithic pottery samples (n=21) and clay samples (n=20) showing Zr/Rb-ratio 262
Fig. 311. Tepe 5. Scatterplot of Early Chalcolithic pottery samples (n=21) and clay samples (n=20) showing CaO/Zr-ratio 262
Fig. 312. Tepe 5. Scatterplot of Early Chalcolithic pottery samples (n=21) and clay samples (n=20) showing SiO_2/Al_2O_3-ratio 263
Fig. 313. Tepe 5. Scatterplot of Early Chalcolithic pottery samples (n=21) and clay samples (n=20) showing SiO_2/K_2O-ratio 263
Fig. 314. Tepe 5. Scatterplot of Late Bronze Age pottery samples (n=8) and clay samples (n=20) showing Sr/Rb-ratio 264
Fig. 315. Tepe 5. Scatterplot of Late Bronze Age pottery samples (n=8) and clay samples (n=20) showing CaO/Sr-ratio 265
Fig. 316. Tepe 5. Scatterplot of Late Bronze Age pottery samples (n=8) and clay samples (n=20) showing SiO_2/Al_2O_3-ratio 265
Fig. 317. Tepe 5. Scatterplot of Late Bronze Age pottery samples (n=8) and clay samples (n=20) showing Sr/Pb-ratio 266
Fig. 318. Tepe 5. Scatterplot of Early Iron Age pottery samples (n=18) and clay samples (n=20) showing Rb/Sr-ratio 267
Fig. 319. Tepe 5. Scatterplot of Early Iron Age pottery samples (n=18) and clay samples (n=20) showing CaO/S-ratio 268
Fig. 320. Tepe 5. Scatterplot of Early Iron Age pottery samples (n=18) and clay samples (n=20) showing SiO_2/Al_2O_3-ratio 268
Fig. 321. Tepe 5. Scatterplot of Early Iron Age pottery samples (n=18) and clay samples (n=20) showing SiO_2/Al_2O_3-ratio after removing CaO from the calculation 269
Fig. 322. Tepe 5. Scatterplot of Early Iron Age pottery samples (n=18) and clay samples (n=20) showing CaO/Sr-ratio 269
Fig. 323. Tepe 5. Scatterplot of Early Iron Age pottery samples (n=18) and clay samples (n=20) showing Sr/Pb-ratio 270
Fig. 324. Tepe 5. Scatterplot of Early Iron Age pottery samples (n=18) and clay samples (n=20) showing Cr/Zn-ratio 271
Fig. 325. Tepe 5. Scatterplot of Early Iron Age pottery samples (n=18) and clay samples (n=20) showing CaO/SiO_2-ratio 271
Fig. 326. Tepe 5. Scatterplot of Late Antique pottery samples (n=3) and clay samples (n=30) showing Sr/Rb-ratio 272
Fig. 327. Tepe 5. Scatterplot of Late Antique pottery samples (n=3) and clay samples (n=30) showing V/Cr-ratio 273
Fig. 328. Tepe 5. Scatterplot of Late Antique pottery samples (n=3) and clay samples (n=30) showing Cu/Zn-ratio 273
Fig. 329. Tepe 5. Scatterplot of Late Antique pottery samples (n=3) and clay samples (n=30) showing CaO/Zr-ratio 274
Fig. 330. Tepe 5. Scatterplot of Late Antique pottery samples (n=3) and clay samples (n=30) showing SiO_2/Al_2O_3-ratio 274
Fig. 331. Tepe 5. Scatterplot of Late Antique pottery samples (n=3) and clay samples (n=30) showing SiO_2/K_2O-ratio 275
Fig. 332. Tepe 5. Scatterplot of Late Antique pottery samples (n=3) and clay samples (n=30) showing Cl/S-ratio 275
Fig. 333. Ratio of hardness and grain size of the analysed samples according to their dating 277
Fig. 334. Tepe 5. Scatterplot of Early Chalcolithic (n=21), Late Bronze Age (n=8), Early Iron Age pottery samples (n=18) and clay samples (n=20) showing Rb/Sr-ratio 279
Fig. 335. Tepe 5. Scatterplot of Early Chalcolithic (n=21), Late Bronze Age (n=8) and Early Iron Age pottery samples (n=18) as well as clay samples (n=20) showing S/Cl-ratio 279
Fig. 336. Tepe 5. Scatterplot of Late Bronze Age (n=8) and Early Iron Age pottery samples (n=18) as well as clay samples (n=20) showing Rb/Sr-ratio 280
Fig. 337. Map of obsidian sources (after Chataigner/Gratuze 2014: Fig. 1) 282
Fig. 338. Tepe 5. PCA of obsidian artefacts (n=48) and source regions (n=37) 283
Fig. 339. Tepe 5. Scatterplot of obsidian artefacts (n=48) and sources (n=37) showing Zr/Sr-ratio 283

Fig. 340. Tepe 5. Scatterplot of obsidian artefacts (n=48) and sources (n=17) showing Zr/Sr-ratio 285
Fig. 341. Tepe 5. Scatterplot of obsidian artefacts (n=48) and sources (n=34) showing Zr/Rb-ratio 285
Fig. 342. Tepe 5. Scatterplot of obsidian artefacts (n=48) and reference material (n=37) showing Nb/Y-ratio.....286
Fig. 343. Tepe 5. Scatterplot of copper (n=5), arsenic copper (n=13), tin bronze (n=17) and leaded tin bronze artefacts (n=1) showing Zr/Sr-ratio 289
Fig. 344. Percentage of metals identified at Tepe 5 289
Fig. 345. Tepe 5. Scatterplot of copper (n=5), arsenical copper (n=13), tin bronze (n=17) and leaded tin bronze artefacts (n=1) showing Ni/Sb-ratio..... 290
Fig. 346. Tepe 5. Scatterplot of copper (n=5), arsenical copper (n=13), tin bronze (n=17) and leaded tin bronze artefacts (n=1) showing Cu/Sn-ratio..... 290
Fig. 347. Tepe 5. Scatterplot of copper (n=5), arsenical copper (n=13), tin bronze (n=17) and leaded tin bronze artefacts (n=1) showing Sn/Pb-ratio 291
Fig. 348. Tepe 5. Scatterplot of copper (n=5), arsenical copper (n=13), tin bronze (n=17) and leaded tin bronze artefacts (n=1) showing Fe/Cu-ratio 291

List of Tables

Table 1. Types of vessels attested in each of the Chalcolithic contexts 19
Table 2. General features and orientation of grave-pits and skeletons of Late Bronze/Early Iron Age burials 37
Table 3. Type and number of objects found in Late Bronze/Early Iron Age burials and in their fill 38
Table 4. Radiocarbon dates of Late Bronze/Early Iron Age burials 39
Table 5. General features and orientation of grave-pits and skeletons of Late Antique burials 43
Table 6. Type and number of objects found in Late Antique burials and in their fill 44
Table 7. Radiocarbon dates of Late Antique burials 45
Table 8. General features and orientation of grave-pits and skeletons of Late Antique burials 48
Table 9. Burials of the Medieval period with burial gifts 50
Table 10. Radiocarbon dates of Medieval burials 52
Table 11. Criteria for sex determination of adult and non-adult skeletons 164
Table 12. Overview of the cranial measures including sections of measurement and measurement tools 165
Table 13. Cranial indices calculated from cranial measures 165
Table 14. Overview of the postcranial measures including measurement tools for humerus, radius, ulna, femur, and tibia 166
Table 15. Postcranial indices calculated from postcranial measures 167
Table 16. Summary of determined sex and age of the individuals from Karacamirli sorted by context 203
Table 17. Results of the cranial indices for nine individuals from Karacamirli, where cranial measurements were possible 205
Table 18. Mean (μ) and standard deviation (sd) of the twelve-dimensional craniometry dataset of nine humans from Karacamirli according to GMM clustering performed with three clusters 208
Table 19. Results of GMM cluster analyses on the twelve-dimensional craniometry dataset 208
Table 20. Results of the postcranial Indices for nine individuals from Karacamirli, where postcranial measurements were possible 210
Table 21. Overview of the distribution of the joint status for different joints and vertebrae of all 34 at least adult individuals from Karacamirli 211
Table 22. Overview of the distribution of the status of the bone surfaces (see ch. V.2.1) for different bones of all 34 at least adult individuals from Karacamirli 212
Table 23. Overview of the distribution of the status of the bone surfaces for different bones of all eight infant or juvenile individuals from Karacamirli 213
Table 24. Overview of the archaeological and modern samples from Karacamirli used for stable isotope analysis 221
Table 25. Results of isotope analyses of collagen and apatite for humans, animals and environmental samples from Karacamirli 224
Table 26. Overview of minimum, mean (μ), standard deviation (sd), and maximum isotope value of the analysed isotopic systems for the humans from Karacamirli 225
Table 28. Isotope values (mean μ, standard deviation sd) of the food sources (input data) from Karacamirli 227
Table 27. Diet-adjusted $\delta^{13}C$ and $\delta^{15}N$ values for the human consumers from Karacamirli 227
Table 29. Source contributions (minimum, mean, maximum) for the individuals from Karacamirli calculated with SISUS using eight food sources (see Table 27 and Table 28) 229
Table 30. Results of GMM cluster analyses with five and six isotopic dimensions 233
Table 31. Mean (μ) and standard deviation (sd) of

the five-dimensional isotopic dataset of the humans from Karacamirli according to GMM clustering performed with two clusters 235
Table 32. Mean (μ) and standard deviation (sd) of the six-dimensional isotopic dataset of the humans from Karacamirli according to GMM clustering performed with two clusters 235
Table 33. Mean (μ) and standard deviation (sd) of the six-dimensional isotopic dataset of the humans from Karacamirli according to GMM clustering performed with two clusters 235
Table 34. List of chemical values of the clay samples discussed in this study 253
Table 35. List of discussed chemical values of the sampled ceramics in this study 258
Table 36. System of ceramic ware codes 277
Table 37. List of sampled obsidian from Tepe 5 284
Table 38. Measurement results of significant elements for the metal artefacts of Tepe 5 and a stray find from the survey (0007) 288

Preface

The Tepe 5 north of the village of Qarajamirli is a small site of less than 0.2 ha, but the cemetery on its top neatly encompasses remains from almost all occupational periods documented up to now in the micro-region south of the Yenikand reservoir in western Azerbaijan. The relevance of the investigations reported on here therefore belies the small number of burials investigated: It provides us with a corpus of dated and analysed material which ideally complements the data collected in our larger project, the Karacamirli survey.

This volume contains the results of a concerted effort which extended over the past 5 years. It started with fieldwork in the years 2015–2017, continued with the subsequent analyses carried out in Baku and Munich between 2018 and 2019 and culminated in the writing and editing process which took another 18 months. As all group efforts tend to do, work on Tepe 5 has brought out the best and worst in the people involved. The exhilarating moment of discovery triggers the excavators as much as popular imagination, but there follows a phase when that beautifully preserved vessel or piece of jewellery discovered just before the close of work must be described, dated, discussed and contextualised, when different strands of information (some of them contradictory!) must be reconciled and synthesized. Now that the results are ready to be published, I am happy to admit that the major efforts were other peoples' – mostly the individual authors' –, and that bringing together the various chapters was the least effort of all, and probably the most pleasurable.

The privilege of working with a devoted and assiduous team of colleagues from Germany and Azerbaijan is only eclipsed by seeing their efforts come to fruition. My thanks go first and foremost to the people who have contributed to this publication, spending their time and energy, and undoubtedly foregoing other duties, in the process. My most sincere thanks are due to our Azeri colleagues who went out of their way to facilitate the collaborative work at Karacamirli. Dr. Maisa Rahimova, director of the Institute of Archaeology and Ethnography of the Academy of Sciences of Azerbaijan, granted permissions for fieldwork and material analyses and took a keen interest in our progress. Numerous other colleagues helped, not only in the preparation of this volume. Emil Iskenderov and Lachin Mustafaev were, in addition to pursuing their own research programmes, responsible for all facets of organization in the field, and in access to archives and collections in the post-excavation phase. All along, they managed to introduce us to current developments in Azeri archaeology and to impart a lasting impression of selfless collegiality and true hospitality.

Closer to home, Giulio Palumbi (Lyon) kindly checked parts of this manuscript. He and Bertille Lyonnet (Paris) supplied publications unavailable to us and kindly discussed aspects of their work. Most small find drawings are from the hands of Manfred Lerchl (Munich). We thank Simon Trixl for the archaeozoological determination of the animal bones and Alina Alesi (both Munich) for the preparation of the histological samples. M. Mach, B. Seelwald (Munich) and D. Steiniger (Berlin) gave us access to standards for our portable XRF instruments.

All research and analysis on Tepe 5 was funded by grants from the Fritz Thyssen Stiftung, which generously supported us for four years, from 2015 until 2018.

The man who made everything possible is, unfortunately, no longer with us. Academician Ilyas Babaev, head of the Institute of Ethnography and Archaeology's expedition and cooperation partner of a succession of German missions, passed away in December 2017. He is sorely missed and this book, which he anticipated as much as anybody, will be dedicated to his memory.

Kai Kaniuth Munich, July 2020

I. Introduction to the volume

Kai Kaniuth

Archaeological fieldwork along the middle stretch of the Kura river was, until recently, mostly linked to industrial or infrastructural projects. In the southern part of the region, in the foothills of the Lesser Caucasus, it was engineers who initiated excavations of Early Iron Age graveyards which they encountered in the vicinity of their mines or refining plants (Belck 1893). Later, in the 1930s, local schoolteachers were a driving force behind the fieldwork (Hummel 1929; Гуммель 1940). A first concerted effort in the documentation and investigation of archaeological remains started in 1946, flanking the Azerbaijan Soviet Socialist Republic's first major infrastructure project, the building of the Mingachevir dam (Асланов et al. 1959; Казиев 1960; Ваидов 1961).

The toponym Karacamirli commonly refers to a number of archaeological sites located on the southern side of

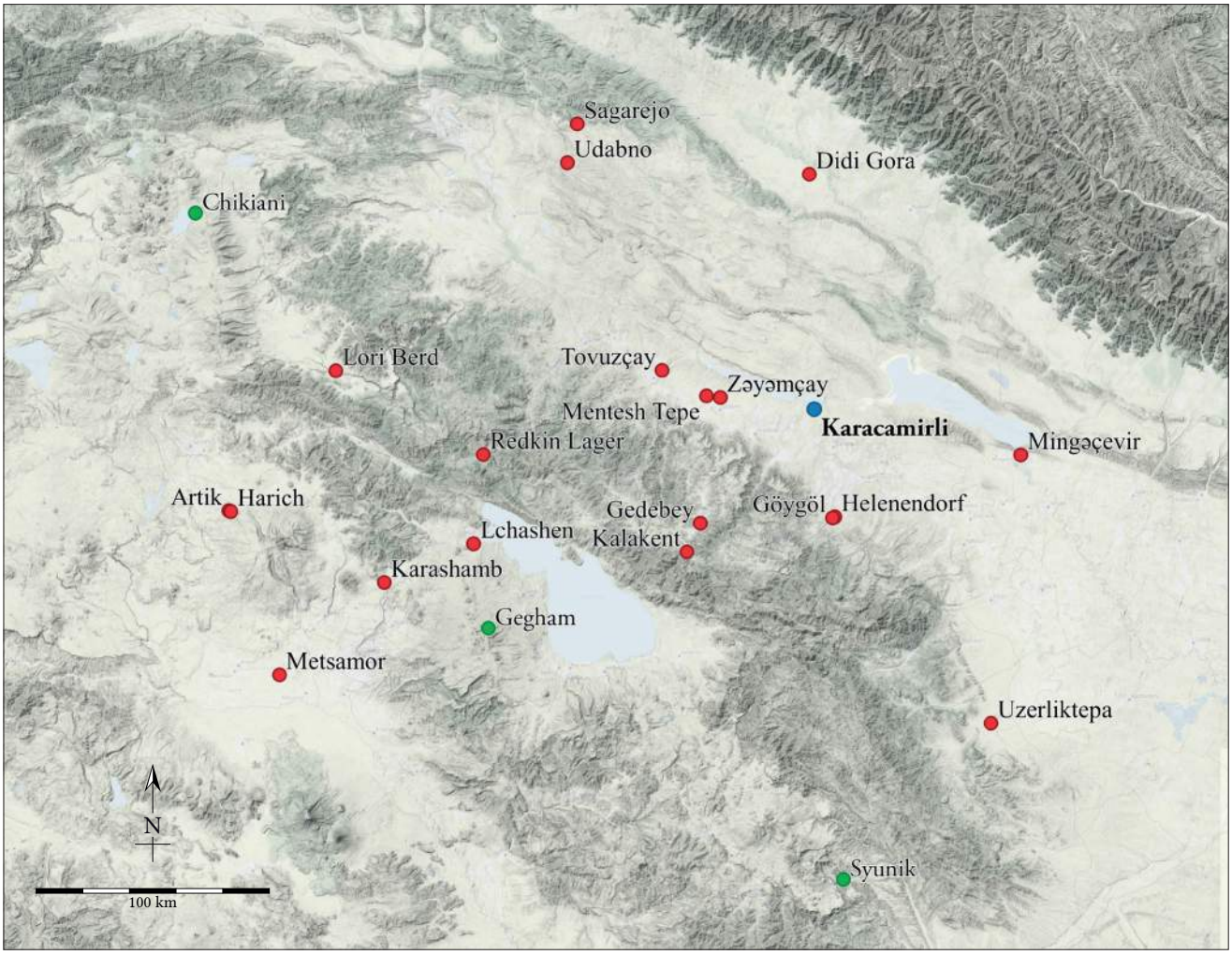

Fig. 1. Archaeological sites (blue and red) and obsidian deposits (green) mentioned in this volume

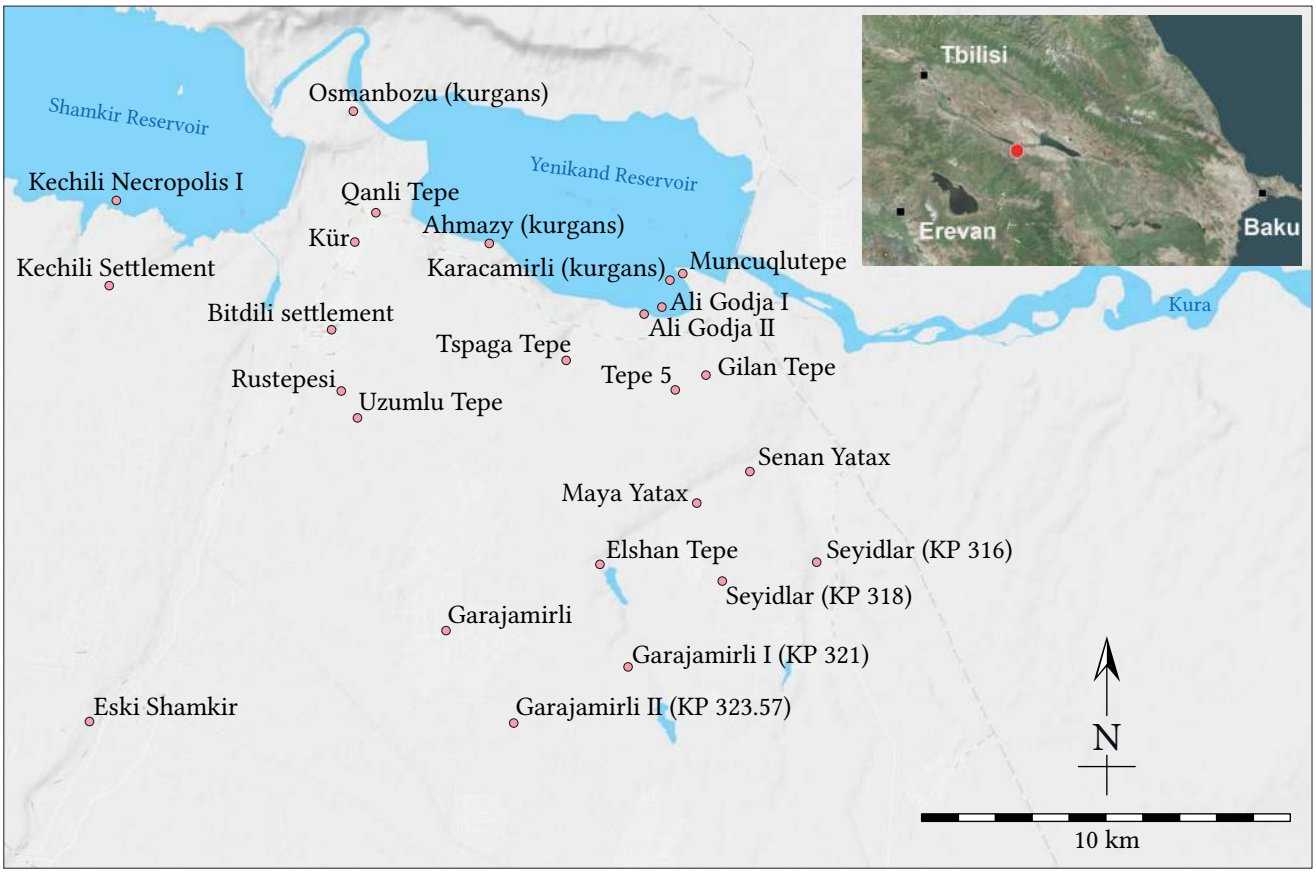

Fig. 2. Archaeological sites north of Garajamirli (basemap: Open Street Map)

the middle Kura valley north of the village of the same name (modern az. Garajamirli/Qaracamirli) in the Shamkir region of the Republic of Azerbaijan (Fig. 1 and Fig. 2).

Systematic archaeological fieldwork in this micro-region began in the early 1970s, when the Shamkir expedition was formed by the Azeri Academy of Sciences' Institute of Archaeology in advance of the construction of the Shamkir dam, designed to use the ponded waters of the Kura river (az. Kür) for use in a hydroelectric power plant above the modern town of Kür. Since 1973, annual work was carried out under the direction of G. P. Kesamanly at several sites, dating from the Chalcolithic until the late Medieval period (Кесаманлы et al. 1976; 1978a; 1978b; Кесаманлы 1981; 2003; Кесаманлы/Джафаров 1977; Джафаров et al. 1982). In the mid-1980s, responsibility for the work was transferred to G. Aslanov and A. Aliev, who shifted their attention further east, where a second, smaller dam was planned near the village of Yenikand (Алиев/Велиев 1986; Алиев 1987; n. d.; Алиев et al. 1988).

The years 2001–2005 saw yet another major infrastructure project, the building of the Baku-Tbilisi-Ceyhan pipeline (BTC). Four sites were discovered near Garajamirli, between kilometres 316 and 323 of the pipeline route, again confirming the general chronological bracket between the Chalcolithic and Middle Ages (Huseynov et al. 2007; Jalilov 2007; Agayev 2006; Dostiyev 2007a).[1]

In 2006, a fourth phase of research started with a joint project by the Institute of Archaeology, Azerbaijan Academy of Sciences (I. Babaev), the Georgian National Museum (I. Gagoshidze) and the Glyptothek and State Collections of Antiquities in Munich (F. Knauss). The aim of their excavations was a suite of Achaemenid period monumental buildings, focusing on the palace of Gurban Tepe (Babaev et al. 2006; 2009; Babaev/Knauss 2010; 2016; Knauss 2007; Knauss et al. 2010; 2013). From 2006–2019, annual campaigns were carried out by the team, documenting the virtual identity of the structure's dimensions with the Hadiš of Xerxes on the Persepolis terrace. The discovery of a spectacular residential and administrative complex, modelled in every respect on an imperial Achaemenid prototype, is at the heart of Karacamirli's international renown today.

1 For the results of the BTC project in general see Taylor/Maynard 2011, Taylor et al. 2011 and Taylor 2018 (for Azerbaijan) and Gamkrelidze 2010 (for Georgia).

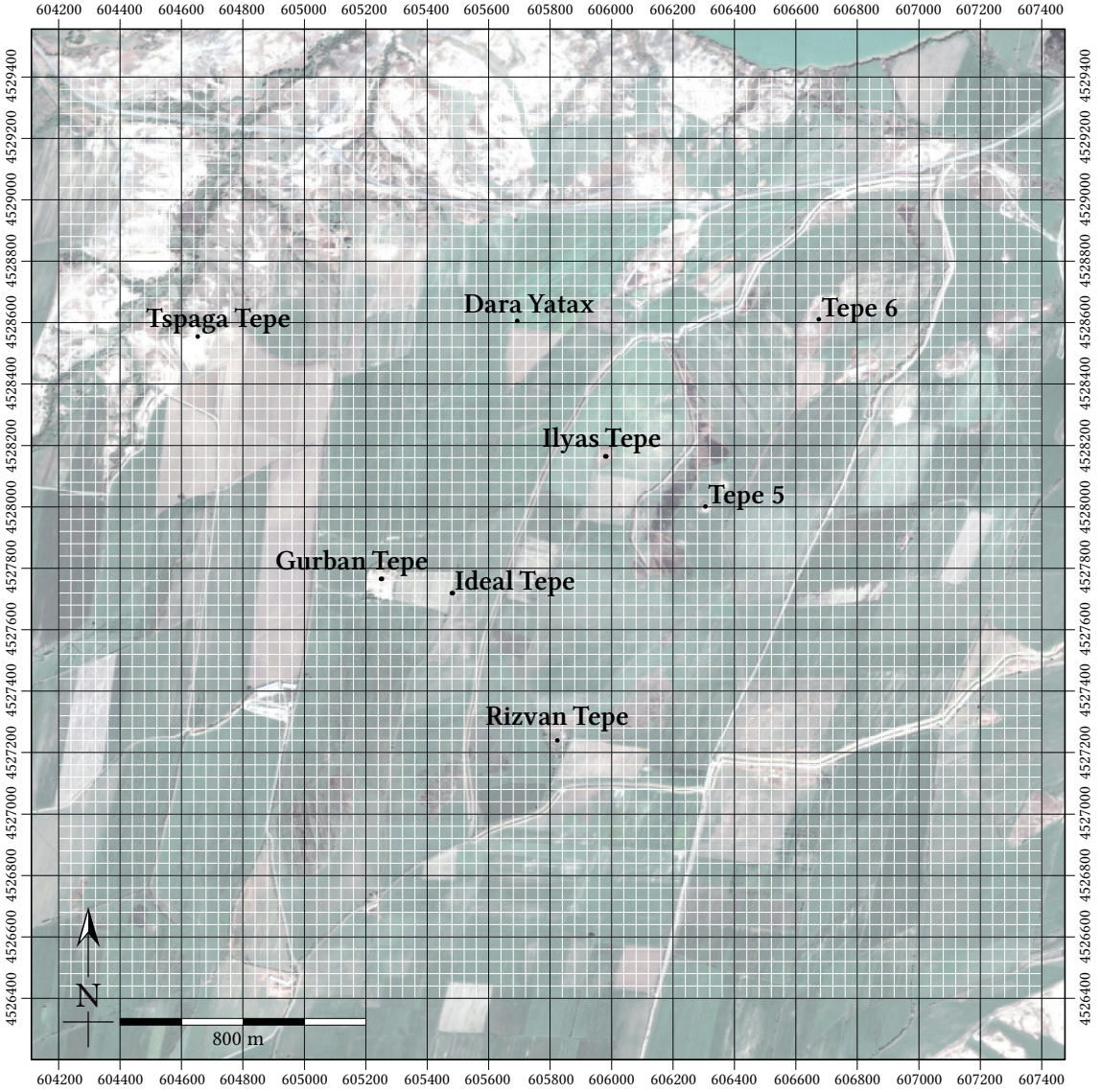

Fig. 3. The Karacamirli survey grid showing Tepe 5 in relation to Gurban Tepe and other archaeological sites of Karacamirli (map base: Quickbird, April 12, 2007)

The desire to study the Achaemenid complex in depth and to situate it within the local settlement history led to the conception of the Karacamirli survey. This project was carried out in cooperation of the Academy of Sciences (I. Babaev) and this author, as representative of Ludwig-Maximilians-University Munich. Funded by the *Deutsche Forschungsgemeinschaft* (DFG Az. KA2288/3, 2013–2014. KA2288/4, 2017–2018) and the *Fritz- Thyssen-Stiftung* (Thyssen-Stiftung Az. 10.14.2.053, 2015– 2018) an intensive surface survey led to the discovery of a number of new sites, the localisation of others, previously known only from short preliminary reports, and, above all, the clarification of the spatial structuration of an Achaemenid centre in the periphery of the empire (Babaev et al. 2016; 2017a; 2017b; Babaev et al. in print). While our research consisted mostly of surface survey work, several excavations were undertaken along. One of these is dealt with in this report.

I.1 The site of Tepe 5

Tepe 5 lies in the eastern part of the Karacamirli survey grid, at 606300.8 E/4527994.3 N (WGS 84, UTM 38N) (Fig. 3).[2] The terrain slopes down from south-east to north-

2 In the early phases of their project, the team of Babaev and Knauss numbered the hitherto unknown sites in the Karacamirli area. Thus, the propylon of the palace complex was labelled Tepe 1



Fig. 4. Location of Tepe 5 on a satellite image (© Quickbird, April 12, 2007)

west, where a small ditch visually and physically separates the site from the Achaemenid occupation further west. Surrounded by modern fields, the tepe forms the second of a row of originally at least four small elevations strung out in north-south direction (Fig. 4). The remaining three have been ploughed under, but were still visible on satellite imagery as late as 2007.

Today, Tepe 5 measures 35 × 40 m. It is a rectangular mound, whose edges have been somewhat cut and straightened by decades of ploughing. Even though some attempts are visible to level the site with the surrounding fields, the elevation still stands some 2.5 m high in its north-western corner (at a max. height of 174.18 m a.s.l.), while in the southeast it rises barely above the cultivated ground. The natural soil of Tepe 5 differs from that of the nearby fields. It is of lighter shade, and harder to work. While we have not undertaken a geomorphological identification, it appears that Tepe 5, like the other three hillocks visible on Fig. 4, and like another, smaller hill west of the ditch, are relicts of an underlying geomorphological stratum which was selected, for one reason or another, as a focus of human activity.

The area around Tepe 5 was included in our survey on 24 September 2015 as part of grid numbers Z41 (6280/7960) and Z53 (6280/8000). The topography of the site stood out, as did the finds collected on the surface nearby (among them a bronze dagger (Fd. no. 0007, picked up 45 m northeast of the tepe), i. e., between Tepe 5 and the next relict tepe. This, of course, opens the possibility that the ancient burial ground may have been considerably larger. The ceramic material was inconspicuous.

The geophysical survey, on the other hand, showed more tangible results and suggested the hill as a very

(later: Ideal Tepe), the palace itself Tepe 2 (later: Gurban Tepe), and the administrative sites in the periphery Tepes 3 (Rizvan Tepe) and 4 (Ilyas Tepe). Only Tepes 5 and 6 – a medieval site several hundred meters to the north (Babaev et al. in print) – retain their original names.

promising location for a detailed investigation. At that time, in late 2015, the nature of the pre-modern use of Tepe 5 was very much open to debate. The regular pattern of the anomalies visible on the magnetometer image (see ch. II) made the presence of a built structure as likely as any other. Our excavations began in the following summer with the only certainty, that conditions and archaeological remains promised to be much different from any other we were likely to encounter in the surroundings of Gurban Tepe.

Since our excavations in the years 2016 and 2017 have provided much more detailed information, a discussion of the survey results – including the comparison of survey and excavation data – will be deferred to the final publication of that work package.

The excavation of Tepe 5 began on the 3rd of August and lasted until the 27th of August 2016. A surface area of 140 sqm was opened in this year in three trenches (Babaev et al. in print). In the following year, the investigations were resumed from 24th of July until 18th of August 2017. Work was carried out by two to three archaeologists and up to 14 workmen from the town of Kür.[3] The excavation was carried out with the help of a Leica TC407 Total Station, within a grid staked out by a GS10 GNSS system. Archaeological deposits were recorded in a single context-system. Contexts numbers consist of three digits preceded by KG (for *Karacamirli Grabung*, i. e. KG-999), small finds, sherd lots, skeletons and samples are identified by a four-digit code (KG-[context]-8888). Individual sherd numbers are listed with reference to the sherd lot-numbers.[4] A Filemaker© database was used to enter the form-based in-field documentation. In the field, no drawings were made. Instead, all visual documentation was photographic, and of all features three-dimensional models were created employing Structure from Motion (SfM) with Agisoft Metashape©. Subsequent to the excavation, the interpretation of remains involved the creation of vector graph plans and drawings. Starting with the 2017 campaign, a portable XRF instrument, Niton XL3t, was used extensively in the Karacamirli project, and a substantial number of finds from Tepe 5 were analysed.[5] In the same year, the anthropological material from both campaigns was studied. A number of samples were exported to Germany for isotope analyses.[6]

I.2 The organization of the present volume

The present volume is the final report on our excavations at Tepe 5. It therefore discusses all parts of our work exhaustively, presenting the entirety of relevant data gathered. The first results obtained at the site will be reported by Jörg Fassbinder and his team, who opened our investigations in the year 2015 with their geophysical prospection (ch. II). Next, Martin Gruber publishes the excavations results, contexts and small finds, which were documented under his supervision (chs. III and IV). Andrea Göhring, who joined our team in 2017, then deals with all aspects of the anthropological remains (ch. V), followed by a report on isotope analyses carried out on the human bone material (ch. VI). Michaela Schauer covers the material science aspects of the Tepe 5 finds (ch. VII), carried out within the larger analytic program run at Karacamirli. Finally, an overview is provided summarising the most important results of our work (ch. VIII).

3 In 2016, the excavation staff consisted of M. Gruber (site supervisor, Munich University), M. Uehara, S. Forstreuter (archaeologists), R. Aliev, H. Aliev, E. Mamedov, Farid Aliev, Fariz Aliev, V. Cəfərov, C. Hüseynov, T. Jusifov, E. Cafarov, C. Qafarov, Z. Məhərrəmov, R. Ahmedov, N. Abdullaev, S. Amiraslanov, E. Bajramov, A. Musayev, S. Namazov, V. Pirverdiev, T. Gasimov, A. Akbarov, S. Askarov, S. Ələkbərov, N. İmamverdiyev and E. Ağayev (workmen). In 2017 M. Gruber was again in charge, aided by M. Uehara, E. Güneş, A. Rybalchenko (archaeologists), N. İmamverdiyev, Z. Məhərrəmov, F. Abdullayev, S. Ələkbərov, N. Abdullayev, C. Ələkbərov, E. Əliyev, E. Mamedov, A. Pənahov, Y. Alnağıyev, A. Həsənov, M. Abdullayev, Q. İmamverdiyev, N. Şahbazi, A. Paşayev, S. İmamverdiyev, A. Mehdiyev, V. Pirverdiyev, M. İbrahimov, E. Ağayev, G. Mamedov, M. Ağayev, A. Süleymanov, A. Musayev, V. Cəfərov, F. Chernasov, N. Seyidov, V. Gasimov, M. Mamedov, V. Aslanov and E. Bogrov (workmen).

4 Hence, KG-010-2222-03 would refer to the third sherd of lot 2222, belonging to context 010.

5 For details concerning the analytic protocol see M. Schauer, in this vol.

6 See Göhring and Göhring et al., in this vol.

II. The Geophysical Prospection around Tepe 5

Jörg W. E. Fassbinder / Florian Becker / Andrei Asăndulesei

II.1 Introduction

Karacamirli, a major Achaemenid palatial structure, has been under excavation since 2006 by F. Knauss and I. Babaev (Babaev et al. 2016; Knauss et al. 2013). From 2013–2017 a systematic archaeological survey combined with a large-scale magnetometer prospection undertaken by Kai Kaniuth and Jörg Fassbinder (Ludwig Maximilians University, Munich) followed up these ground-breaking studies by considering patterns of land use and the spatial structuration of an Achaemenid imperial site.

According to the ceramic finds, the area of Karacamirli was occupied from the Chalcolithic period until the Middle Ages. The intensive archaeological survey target-

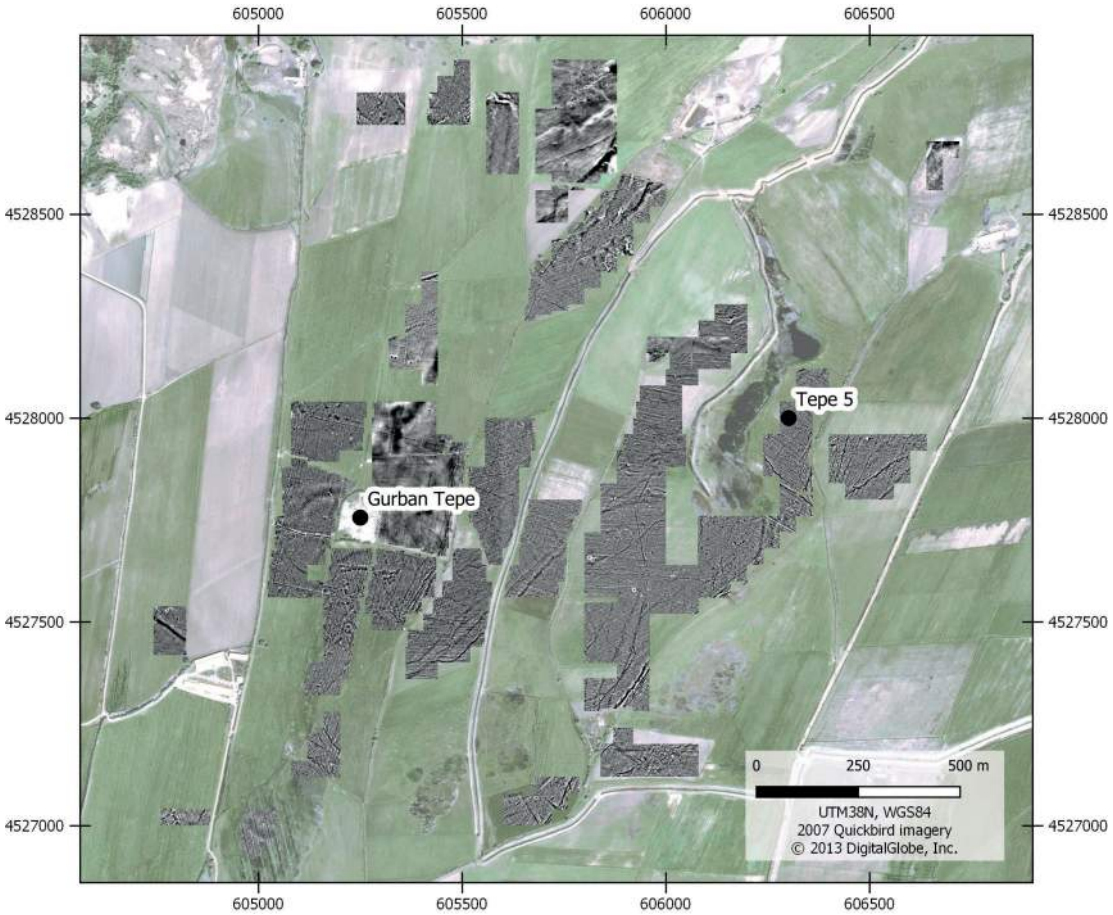

Fig. 5. Karacamirli. Satellite overview of the total area overlaid by the grey scale images of the magnetometer survey areas. The grey scale patchwork is due to the application of different instruments (caesium and fluxgate magnetometer) with different sensitivities/dynamics (Quickbird imagery © 2013 DigitalGlobe from April 12th, 2007)

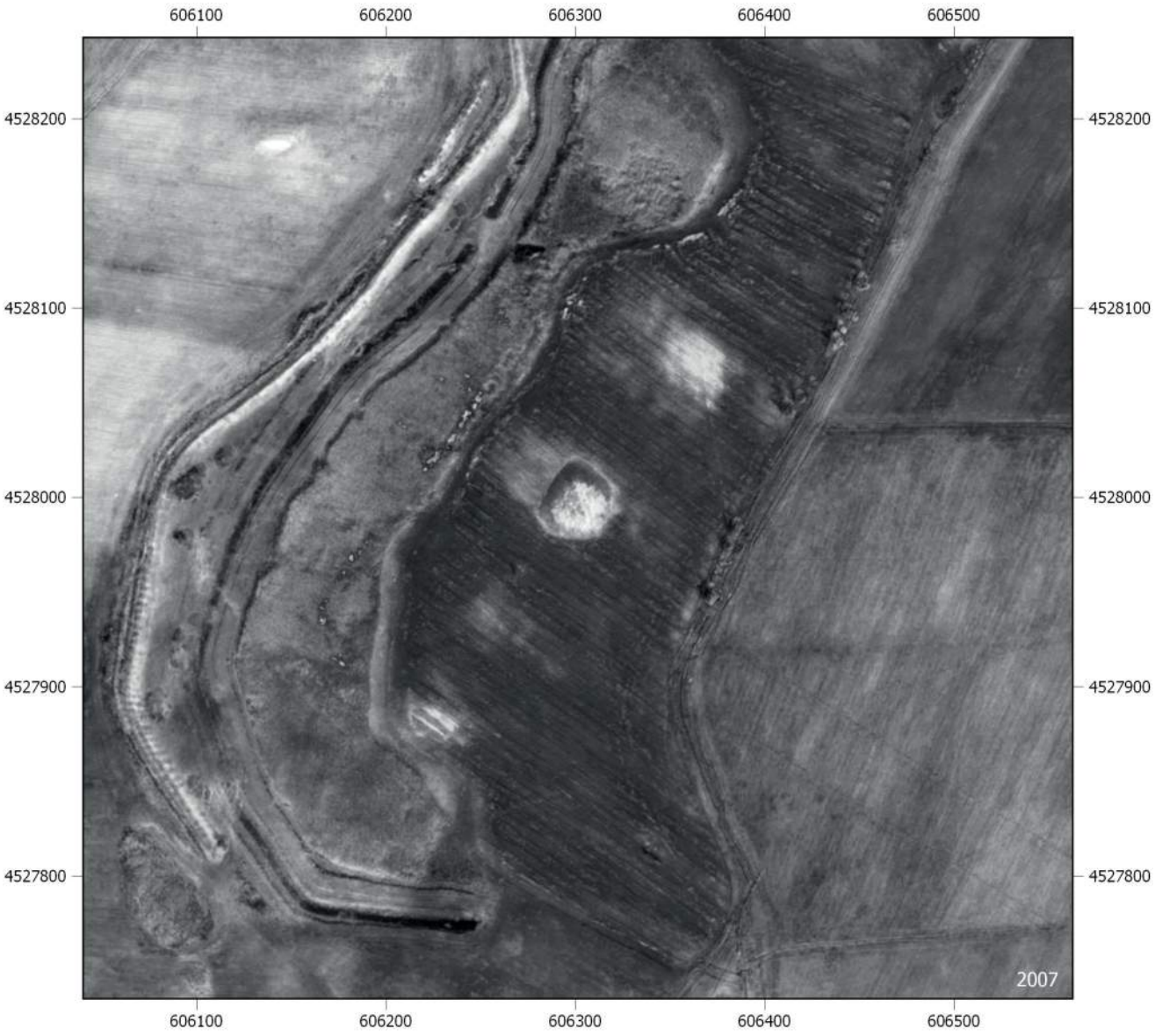

Fig. 6. Karacamirli. Tepe 5 area: Quickbird satellite image from April 12th 2007 (© 2013 DigitalGlobe); WGS 84 UTM 38N

ed an area of c. 4 km², of which more than 1.5 km² were prospected by a magnetometer survey (Fig. 5).

Our first tests for the suitability of magnetometer prospecting in 2013 were undertaken with the Scintrex SM-4G-Special caesium magnetometer to prove the feasibility of the site for geophysical prospection. In three field seasons from 2015–2017 we applied all our disposable magnetometers (fluxgate and caesium magnetometers) to cover all accessible areas adjacent to the palace and in its periphery.

For this purpose, we worked with several teams and applied two 4-sensor (Förster-Ferex) fluxgate magnetometer units and two Caesium-magnetometers. The prospecting areas were selected according to their accessibility and suitability for a high-resolution magnetometer prospection. All these areas were scanned with a sampling interval of 10 × 50 cm.

For a better understanding, the magnetometer measurements were complemented by Earth Resistance Tomography (ERT) measurements, susceptibility measurements, some trial excavations and additional mineral magnetic analyses of archaeological soils and typical soil layers. The results of this part of the project will be published in a separate report.

Apart from the known sites which had formed part of the Achaemenid administrative centre, geophysics were employed predominantly, whenever noteworthy topographic features, remote sensing data or concentrations of ceramic finds indicated sub-surface archaeological structures. All of this was the case at Tepe 5.

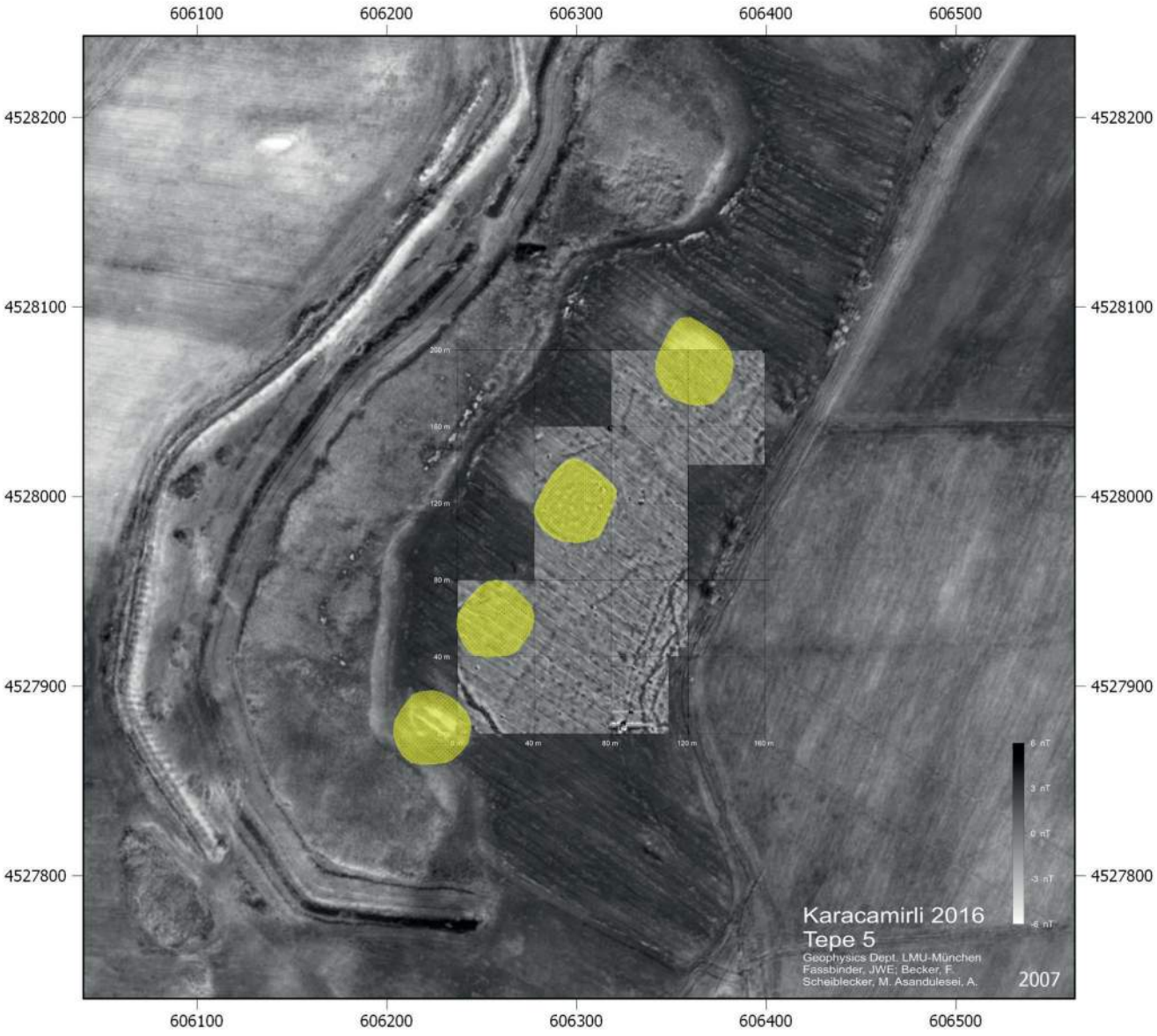

Fig. 7. Karacamirli. Tepe 5 area: Quickbird Satellite image from 2007 (© 2013 DigitalGlobe), overlaid by the magnetogram of the area. The location of former and still existing mounds is marked in yellow; WGS 84 UTM 38N

II.2 The Geophysical Prospection of Tepe 5

The mound named »Tepe 5«, is situated c. 1200 m northeast of Gurban Tepe. It is visible on vintage CORONA and more recent Quickbird satellite images (Fig. 6) which show a more or less regular row of four white spots in this area, indicating burial mounds or other undated archaeological sites. Three of these sites were already intensively ploughed and hence invisible from the ground. Only one mound appeared fairly untouched. It forms a square shaped elevation of c. 2.5 m height and c. 40 m diameter. Previous to our measurements nothing was known about the constitution, composition or the function of this site. The controlled sherd pickup did demonstrate, however, that we were dealing with an archaeological site.

The mound, so far excluded from modern farming, was overgrown by high grass and bushes. We prepared the area for the magnetometer prospection manually by cutting and clearing the vegetation. While the periphery and the area adjacent to the mound had already been measured with a fluxgate magnetometer, we decided to survey the mound itself with a more sensitive caesium magnetometer (Geometrics G-585) in duo-sensor configuration. Caesium magnetometers usually have five times higher intensity anomalies than gradiometers which allows an insight to deeper soil horizons (Linford et al. 2007; Mathé et al. 2009; Fassbinder 2015).

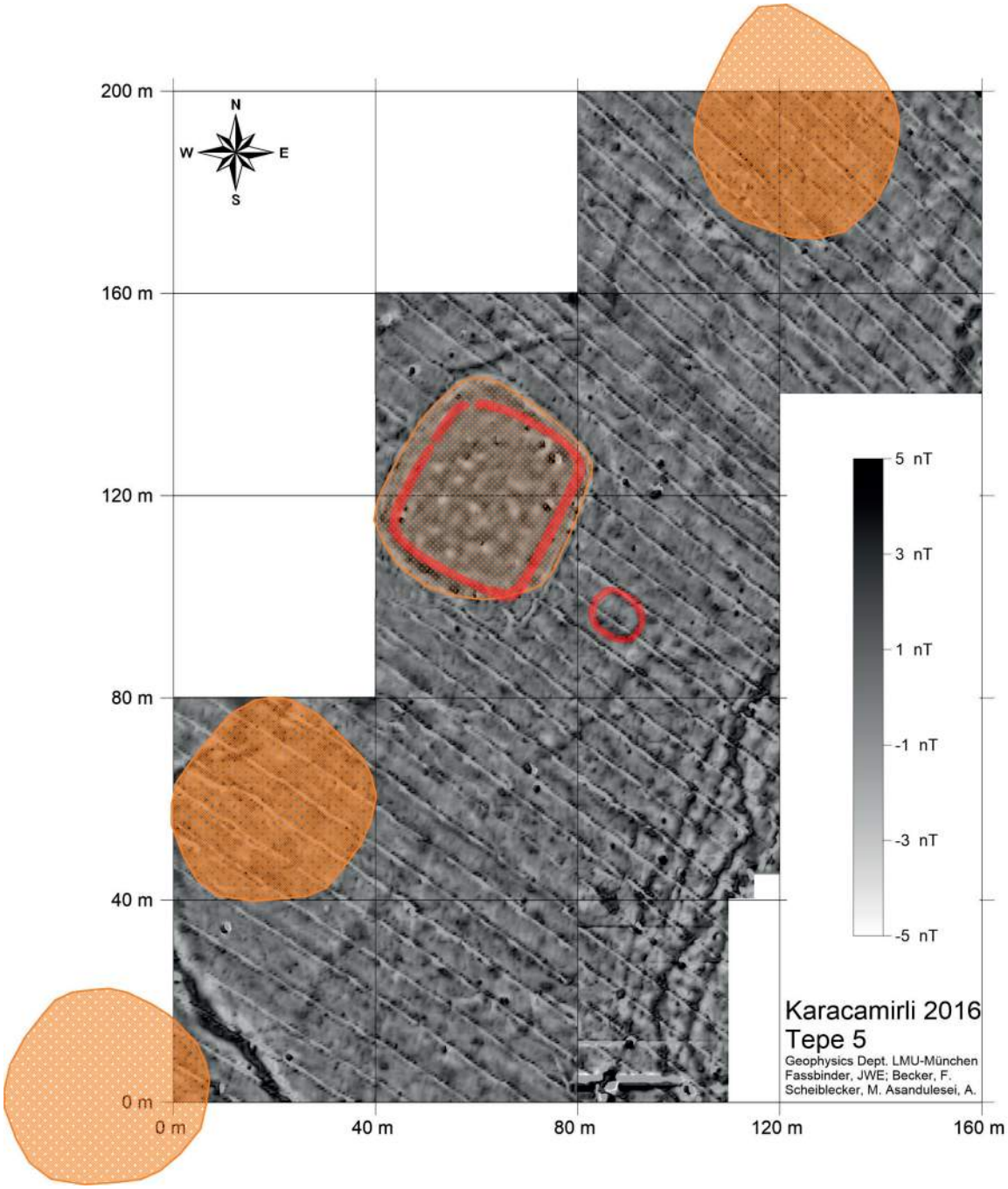

Fig. 8. Karacamirli. Tepe 5 and its surroundings: Magnetogram of the burials and mounds, the »inner enclosure« and its periphery. Caesium total field magnetometer (Geometrics, G-585 in duo-sensor variometer configuration) in the area on top of the mound and Ferex Foerster (four sensor fluxgate gradiometer) applied in the periphery of the mound. Sampling density 12.5 × 50 cm resp. 10 x 50 cm, interpolated to 12.5 × 12.5 cm, dynamics ±15 resp. 3 nT fused to ±4 nT in 256 grey-scales, 40 m grid

Analysing the magnetogram in detail, we believe that the inner structure of the mound forms a rectangle with rounded edges, c. 35 × 25 m in size. The longer side is tilted clockwise by c. 27°. The mound itself was never touched by modern farming. Irrigation canals and ploughmarks are only visible around the mound. Possibly, the agricultural activity is in part responsible for the rhomboid shape of the hill. The periphery of the mound, like the predominant part of the landscape in Karacamirli (see magnetograms in Fig. 5), is seriously disturbed by modern irrigation canals, which run parallel to each other at a distance of 5 m. They are c. 30 cm wide and incised c. 20–30 cm deep into the ground. Due to their short distance to the magnetometer probes during the

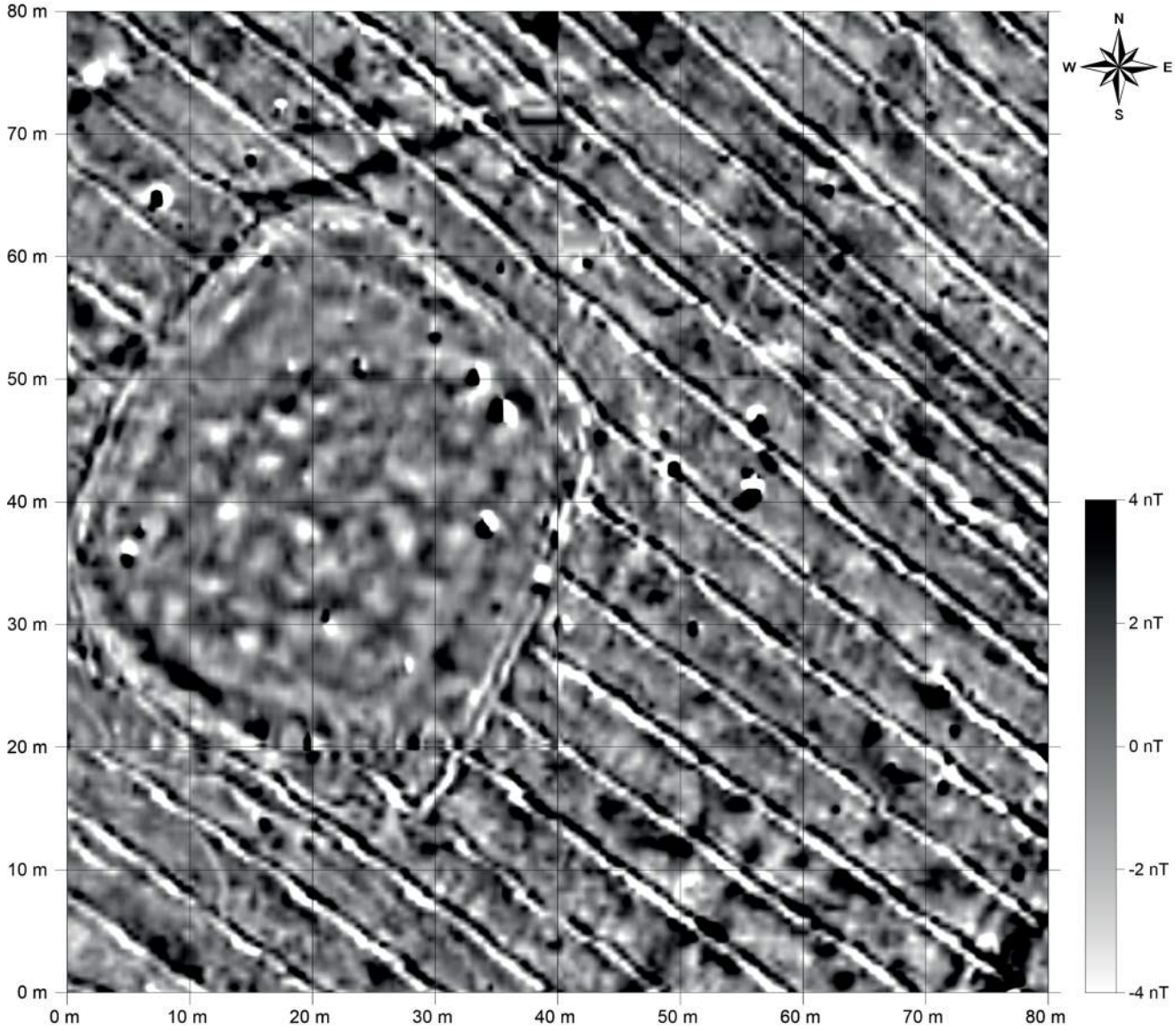

Fig. 9. Karacamirli, Tepe 5. Detail of the magnetogram with the burial mound. Notice that the magnetic anomalies of the pits on top of the mound are positive and negative; while in the periphery these are almost only positive ones (for technical details see Fig. 8)

survey these features show up very sharply and obscure the image as from a window blind.

The magnetogram clearly indicated the presence of non-natural subsurface structures on the mound. At first sight it appeared to conform to the ground plan of a massive building complex (Fig. 8 and Fig. 9). The more or less regular pattern of »negative« white anomalies led us to the assumption that we had discovered a monumental building complex possibly linked functionally to the administrative complex centred on Gurban Tepe.

Comparing our first geophysical assessment, the excavation and discovery of a cemetery therefore came as a surprise. On the other hand, previous measurements of burial grounds and cemeteries elsewhere show similar results with burial pits showing up as negative (white) anomalies (Fassbinder et al. 1999; Fassbinder/Becker 2003; Fassbinder 2017).

The burials on the mound seem to be arranged as within an »enclosure«, oriented by c. 27° towards the north-east. The burials here show up as negative and positive magnetic anomalies. Together they form a square shaped pattern of burial pits, which is enclosed by a linear feature. Within this rectangular structure with rounded edges, was the trace of a palisade, a ditch or a wall of rammed earth, the nature of which cannot be determined solely by the magnetic image. Extensive agriculture deformed the mound already and gives it its rhomboid shape (Fig. 10 and Fig. 11).

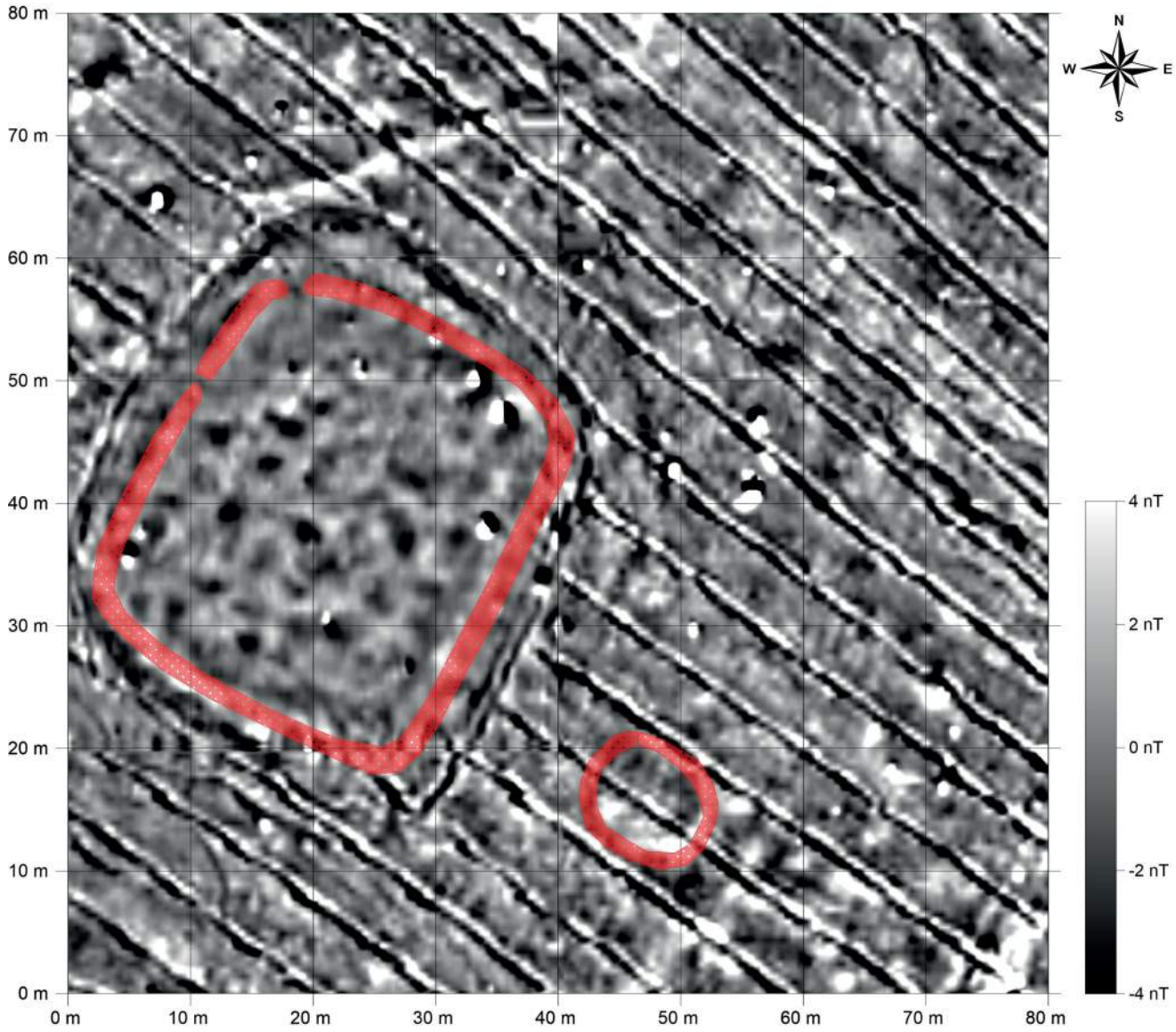

Fig. 10. Karacamirli, Tepe 5. Detail of the magnetogram (like Fig. 5, but with inverted greyscale). The layout of the presumed enclosure is marked in red

Whether burials show up as »positive« (= black) or as »negative« (= white) anomalies, depends on the magnetic susceptibility of the infill and the demagnetized natural remanent magnetization of the adjacent sediments in the burial pit. In the area of the mound, we detect both types; however, both are similarly arranged (see Fig. 9 and Fig. 10). South-east of the mound, we detect another enclosed feature with pits inside. Such features are reminiscent of Iron Age kurgan sites in the Northern Caucasus, the Volga steppe and Kazakhstan (Gass et al. 2019; Парцингер et al. 2018). In addition to this small enclosure, a multitude of other pits of more or less of similar size are discernible to the east of Tepe 5. Nearly all of them show positive anomalies. We therefore suggest that these pits could be further burials and that the whole area represents a large cemetery. Usually, pits of a settlement should come in different sizes, shapes and diameters. Linear features, indicating ground plans of houses or buildings, were not detected, but could be still there and overprinted and masked by the sharp and strong traces of the irrigation canals. Even though we consider the presence of a major cemetery very likely, we cannot entirely exclude the possibility that (at least some of) these traces are simply from a settlement.

The question may arise, why there are burial pits with positive and negative anomalies on the mound, but only positive ones in the periphery. The answer probably lies in the different geological background and composition